JOURNAL OF GEOPHYSICAL RESEARCH, VOL. 113, D07205, doi:10.1029/2007JD009019, 2008

Importance of global aerosol modeling including secondary organic aerosol formed from monoterpene

Daisuke Goto,[1] Toshihiko Takemura,[2] and Teruyuki Nakajima[1]

Received 30 May 2007; revised 26 October 2007; accepted 10 December 2007; published 9 April 2008.

[1] A global three-dimensional aerosol transport-radiation model, coupled to an atmospheric general circulation model (AGCM), has been extended to improve the model process for organic aerosols, particularly secondary organic aerosols (SOA), and to estimate SOA contributions to direct and indirect radiative effects. Because the SOA formation process is complicated and unknown, the results in different model simulations include large differences. In this work, we simulate SOA production assuming various parameterizations of (1) primary organic aerosols (POA) mass concentrations, (2) oxidant species concentrations, and (3) volatile organic compound (VOC) concentrations in the SOA formation through gas-to-particle conversion governed by equilibrium partitioning of monoterpene oxidation products. Comparisons of results from observations, other models, and our simulations with/without the SOA partitioning theory lead to some findings of the influence of SOA on the radiation and cloud fields. First, the SOA number concentrations control cloud droplet effective radii near water cloud tops in the tropics and can affect the estimation of the aerosol indirect radiative effect. Second, SOA simulation results strongly depend on POA concentrations and emission data, so that disregarding this dependence may lead to a significant underestimation of the aerosol radiative effect because most of other studies assume that the SOA production level in the preindustrial era is same as in the current level. The global annual mean production of SOA formed from monoterpene is evaluated in this study as 6.74 Tg a^{-1}, and the global annual mean radiative forcings of the direct and indirect effects by SOA from monoterpene are calculated to be -0.01 and -0.19 W m^{-2}, respectively.

Citation: Goto, D., T. Takemura, and T. Nakajima (2008), Importance of global aerosol modeling including secondary organic aerosol formed from monoterpene, *J. Geophys. Res.*, *113*, D07205, doi:10.1029/2007JD009019.

1. Introduction

[2] Aerosol particles, which can scatter and absorb solar radiation, can change the Earth's radiation budget and therefore Earth's climate. This effect is called the aerosol direct effect. Aerosols containing water-soluble compounds act as cloud condensation nuclei (CCN) and can cause changes in hydrometeors and precipitation properties. These are termed as ''Twomey effect'' (or first indirect effect) and cloud lifetime effect (or second indirect effect), respectively [*Twomey*, 1974; *Albrecht*, 1989]. The Twomey effect is the decrease in the cloud droplet effective radius when the aerosol number concentrations increase for constant cloud liquid water and thus increase albedo. The cloud lifetime effect is that the decrease in the cloud droplet radius with increasing aerosols causes a suppression of precipitation and an increase in cloud water.

[3] Carbonaceous aerosols comprise particulate black carbon (BC) and organic carbon (OC). The former can absorb solar radiation, whereas the latter is generally non-absorbing matter. Organic carbon can be further divided into two categories by formation processes: (1) Primary organic aerosols (POA) are directly emitted as particles from biomass burning, fossil fuel combustion, and various other combustion processes; (2) secondary organic aerosols (SOA) are produced in the atmosphere through photo-oxidation of reactive volatile organic compounds (VOC) followed by partitioning or condensation of low volatile products into the aerosol phase [*Seinfeld and Pandis*, 1998]. SOA are formed both from natural sources and from anthropogenic sources. While anthropogenic SOA have large contributions to urban aerosols [e.g., *Takegawa et al.*, 2006], natural SOA have impacts on global aerosols [e.g., *Kanakidou et al.*, 2005], and therefore, SOA need to be evaluated for estimating the aerosol radiative forcing due to human activities after the industrial revolution.

[4] In most general circulation models (GCM), SOA are not treated, or treated very simply, without detailed physical-chemical formation processes, because of limited knowledge and computer resources [*Textor et al.*, 2006]. It is also difficult in modeling to quantify SOA themselves

[1] Center for Climate System Research, University of Tokyo, Kashiwa, Japan.
[2] Research Institute for Applied Mechanics, Kyusyu University, Kasuga, Japan.

0148-0227/08/2007JD009019$09.00

because they are largely unknown compounds and have very complex formation processes, such as partitioning [e.g., *Griffin et al.*, 1999a], heterogeneous reaction [*Jang et al.*, 2002] and in-cloud formation [*Warneck*, 2003]. Despite large uncertainties in the SOA formation pathways, some GCMs include SOA formation schemes, which are mainly divided into two methods: (1) "two product yield model" based on the partitioning theory [e.g., *Griffin et al.*, 1999b] and (2) "explicit chemistry and condensation/evaporation parameterization" [e.g., *Jenkin*, 2004]. Most models assume SOA precursors are monoterpenes and other reactive VOC (ORVOC), as suggested by *Griffin et al.* [1999b], and recently *Henze and Seinfeld* [2006] assume isoprenes are SOA precursors, as suggested by laboratory studies [e.g., *Kroll et al.*, 2005]. These models estimate a global annual SOA production of about 12–70 Tg a^{-1} [*Chung and Seinfeld*, 2002; *Tsigaridis and Kanakidou*, 2003; *Kanakidou et al.*, 2005]. However, they did not focus on the SOA indirect effect, even though some types of SOA are very efficient as CCN because of their hygroscopicity. In addition, because the aerosol indirect effect is sensitive to predicted CCN number concentrations [*Penner et al.*, 2006], it is important to estimate the SOA contributions to CCN.

[5] In this study, we have extended the organic aerosol model in a global three-dimensional aerosol transport-radiation model, Spectral Radiation-Transfer Model for Aerosol Species (SPRINTARS), which simulates mass concentrations and optical properties of tropospheric aerosols (dust, sea salt, organic carbon, black carbon, and sulfate aerosol) [*Takemura et al.*, 2000, 2002, 2005]. In the previous studies with this model they treat SOA very simply as obtained from a conversion rate of biogenic terpene depending on only the seasonal terpene emission distributions of *Guenther et al.* [1995]. This simple parameterization is not adequate because SOA formation depends not only on VOC concentrations but also on oxidants and preexisting organic aerosol concentrations, as determined by many chamber experiments [e.g., *Griffin et al.*, 1999b]. In this paper, we introduce these experimental dependences of SOA formation in the model. In addition, we simulate the cloud droplet effective radii near the top of water clouds, which significantly affects cloud radiative properties, using an aerosol-cloud droplet parameterization based on the Köhler theory for estimation of the aerosol indirect effect [*Takemura et al.*, 2005]. We investigate differences between the cloud radiative property with/without SOA partitioning theory and with a simple SOA parameterization. Then, we compare the results of aerosol direct and indirect effects and estimate the impact of the simulation of SOA formation on the cloud fields. Section 2 provides a description of the present model. Simulation results are presented in section 3, a discussion is presented in section 4, and the conclusions are provided in section 5.

2. Model Description

[6] In this study, we use the global three-dimensional aerosol transport-radiation model, Spectral Radiation-Transport Model for Aerosol Species (SPRINTARS), which is described by *Takemura et al.* [2000, 2002, 2005]; we give only a brief description in this paper. The SPRINTARS has been implemented in an atmospheric GCM developed by the Center for Climate System Research of the University of Tokyo, National Institute for Environmental Studies, and Frontier Research Center for Global Change (hereafter referred to as CCSR/NIES/FRCGC-MIROC AGCM). The horizontal resolution of the triangular truncation is set to T42 (approximately 2.8 by 2.8° in latitude and longitude) and the vertical resolution is set to 20 layers. The time step is set to 20 min. The model predicts the mass mixing ratios of the main tropospheric aerosols, i.e., carbonaceous aerosol (BC and OC), sulfate, soil dust, sea salt, and the precursor gases of sulfate, i.e., sulfur dioxide (SO_2) and dimethylsulfide (DMS). The particles are treated as external mixtures for sulfate, soil dust, and sea salt. For carbonaceous aerosols, the SOA and 50% BC mass from fossil fuel source are treated as externally mixed particles, but other carbonaceous particles are treated as internal mixtures of BC and POA. For soil dust and sea salt aerosols, the mode radii are variable for calculate size bins. On the other hand, for carbonaceous and sulfate aerosols, the dry mode radii are set to 0.1 and 0.0695 μm, respectively [*Takemura et al.*, 2005]. The aerosols densities are set to the same values as *Takemura et al.* [2005]. The aerosol number concentrations are calculated using assumed the aerosol size distributions and the aerosol densities.

[7] The aerosol transport processes include emission, advection, diffusion, sulfur chemistry, wet deposition, and gravitational settling. The radiation scheme, *MSTRN*-8, in the CCSR/NIES/FRCGC-MIROC AGCM can handle scattering, absorption, and emission by aerosol and cloud particles, as well as absorption by gaseous constituents [*Nakajima et al.*, 2000].

[8] All the emission fluxes in 1990, i.e., those of aerosols and their precursors, except a precursor gas of SOA, are those described by *Takemura et al.* [2005]. The precursor gas of SOA is assumed to be biogenic monoterpene ($C_{10}H_{16}$), which is adopted from the Global Emissions Inventory Activity (GEIA) database [*Guenther et al.*, 1995], and the diurnal variation in the emission of biogenic monoterpene is calculated using temperature dependences.

[9] Our aerosol transport schemes except for the SOA treatment are also used by *Takemura et al.* [2005]. Although they assume that SOA production is determined from natural VOC emission by simply multiplying a conversion factor, we introduce a SOA formation scheme controlled by equilibrium partitioning of semivolatile gases [*Pankow*, 1994a, 1994b]. First, these semivolatile products are formed by monoterpene oxidation. Using an off-line chemical transport model, CHASER [*Sudo et al.*, 2002], which has been also implemented in the CCSR/NIES/FRCGC-MIROC AGCM, we calculate monoterpene oxidations with oxidants (OX_j), either ozone (O_3), hydroxyl (OH), or nitrate (NO_3) radicals as follows:

$$C_{10}H_{16} + OX_j \rightarrow \alpha_{i,1}P_{i,1} + \alpha_{i,2}P_{i,2} + \text{others},$$

where $\alpha_{i,j}$ is the stoichiometric coefficient for the lumped category (i) of products (P_i). The two semivolatile gases (P_i) formed by monoterpene oxidation are surrogates for a large number of condensable products, many of which have not been identified in laboratory studies [*Yu et al.*, 1997]. The stoichiometric coefficients and the equilibrium constant K

Table 1. Mass Stoichiometric Coefficient (α) and Equilibrium Constant (K) in Terpene Oxidations

	Terpene + O_3[a,b]	Terpene + OH[b,c]	Terpene + NO_3[a,b]
α_1	0.125	0.038	1
K_1	0.088	0.171	0.0163
α_2	0.102	0.326	0
K_2	0.0788	0.004	0

[a] *Griffin et al.* [1999a, 1999b].
[b] Terpene means alpha-monoterpene in the table.
[c] *Hoffmann et al.* [1997].

are determined by *Griffin et al.* [1999b] and *Hoffmann et al.* [1997], and are shown in Table 1. ORVOC from biogenic compounds are not adopted as SOA precursors.

[10] Monoterpene oxidation products (P_i) are assumed to be partitioned into the aerosol phase because of their polarity and low vapor pressure. Equilibrium between gas and aerosol phases of semivolatile products is given by

$$G_i = \frac{A_i}{K_i M_o}, \tag{1}$$

where A_i and G_i are semivolatile organic compounds (P_i) in aerosol and gas phases, respectively. K_i is the equilibrium constant for the lumped category (i), which depends on temperature according to the Clausius-Clapeyron equation [*Chung and Seinfeld*, 2002; *Tsigaridis and Kanakidou*, 2003], assuming that the enthalpy of vaporization of SOA is 79 kJ mol^{-1} [*Lide*, 2001]. M_o is the total organic aerosol mass concentration in $\mu g\ m^{-3}$ and is given by

$$M_0 = [OA] + \sum_i A_i, \tag{2}$$

where $[OA]$ is a summation of organic aerosol concentrations including POA and SOA and internally mixed BC concentrations before the current time step. SOA concentrations are calculated by solving equations (1) and (2) iteratively [*Chung and Seinfeld*, 2002; *Tsigaridis and Kanakidou*, 2003]. The maximum of iteration number is set to ten. We assume that generated monoterpene products are removed from atmosphere within one time step in our model because they are assumed to be very unstable. And we do not assume reevaporation of these generated monoterpene products from particles. Their treatment is discussed in section 4. In this study, SOA are treated as external mixtures. The reasons are that first the partitioning theory does not give the ratio of condensation/nucleation but gives the SOA mass concentration through both condensation and nucleation. Second, because our AGCM cannot predict the size of the organic aerosol explicitly, it is difficult to simulate the change of the size of organic aerosols by SOA condensation. Third, if we treat SOA as internal mixtures with POA, which are assumed to be composed of five species in our model, we need to set at least five additional tracers for SOA condensation under limited computer resource. We use the SOA dry radius of 80 nm, which is critical for predicting cloud droplet number concentration through our parameterization based on the Köhler theory.

[11] Similar to *Takemura et al.* [2005], we calculate cloud droplet number concentration, cloud water content, and cloud droplet effective radius, for estimating the aerosol indirect effect. Conversion of aerosol number concentrations (N_a) into cloud droplet number concentrations (N_c) is parameterized as by *Ghan et al.* [1997] and *Takemura et al.* [2005]. This N_a-N_c parameterization is based on the Köhler theory as a function of updraft velocity, aerosol chemical composition, and aerosol size distribution. The updraft velocity is given by the sum of grid mean updraft velocity and subgrid updraft velocity using the turbulent kinetic energy [*Lohmann et al.*, 1999; *Takemura et al.*, 2005]. By combining both the cloud liquid water content (l) calculated in the physical frame of the AGCM and the N_c calculated through the present parameterization, the cloud droplet effective radius (R_{eff}) is estimated as follows:

$$R_{eff} = k\left(\frac{3}{4\pi\rho_w}\frac{\rho l}{N_c}\right)^{1/3}, \tag{3}$$

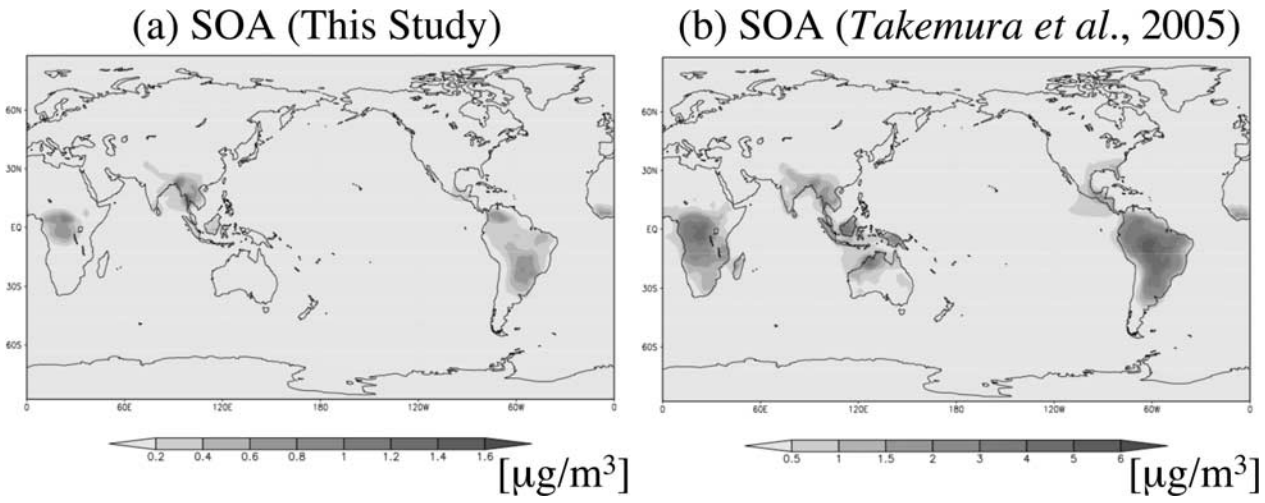

Figure 1. Simulation of SOA mass concentrations near the surface, in February ($\mu g/m^3$), in this study and by *Takemura et al.* [2005].

Table 2. Carbonaceous Aerosol Mass and Total Aerosol Number Concentrations at the Surface in the Amazon Basin Around [10°S, 62°W], During the Wet Season

	Mass[a] (μg/m^3)
Simulations	
This study[b]	2.50
Takemura et al. [2005][b]	6.79
Observations	
Artaxo et al. [2002][c]	2.31
Guyon et al. [2003][d]	0.8967
Decesari et al. [2006][e]	1.42[f]
Hoffer et al. [2006][e]	1.5,[g] 1.8[h]

	Number Concentrations[i] (cm^{-3})
Simulations	
This study[b]	876
Takemura et al. [2005][b]	14694
Observations	
Artaxo et al. [2002][c]	890
Rissler et al. [2006][e]	785,[j] 406,[k] 849[l]

[a]Total carbonaceous aerosol mass concentrations.
[b]In February.
[c]From January to May 1999.
[d]From April to May 1999.
[e]In November 2002.
[f]OC mass concentrations in units of μgCm^{-3}.
[g]During the day average.
[h]During the night average.
[i]Total aerosol number concentrations.
[j]Diurnal averaged accumulation mode (mean diameter = 128 nm).
[k]Diurnal averaged Aitken mode (mean diameter = 61 nm).
[l]Diurnal averaged nucleation mode (mean diameter = 12 nm).

where ρ and ρ_w are the densities of air and cloud water, respectively. The empirical constant k, which is a conversion factor for the effective particle radius depending on the shape of the cloud droplet size distribution, is set to 1.1 for all conditions as suggested by *Martins et al.* [1994]. This R_{eff} is used to estimate the first aerosol indirect effect. In addition, to estimate the second aerosol indirect effect, we considered the influence of the N_c on the cloud liquid water path by changing the precipitation rate. This process is modeled using a parameterization of *Berry* [1967] with parameters set to the same value as in the work by *Takemura et al.* [2005].

[12] The radiative forcing of SOA alone is calculated as the difference in net fluxes with and without SOA under the same meteorological conditions.

3. Results of Numerical Experiments

[13] In this section, we want to compare simulations with/without SOA partitioning theory and also compare the results with observations obtained from field and global satellite measurements. However, there are few field observational reports that specify natural OC and that include natural SOA, except in the Amazon basin, which is one of the largest terpene emission areas [*Guenther et al.*, 1995]. Table 2 compares observations near the surface in the Amazon of both total carbonaceous aerosol mass concentrations and total aerosol number concentrations from simulations with/without SOA partitioning theory [*Artaxo et al.*, 2002; *Guyon et al.*, 2003; *Decesari et al.*, 2006; *Hoffer et al.*, 2006; *Rissler et al.*, 2006]. And Figure 1 shows simulated SOA mass concentrations near the surface in February. During this month of wet season, SOA are assumed to be major components in the Amazon, whereas during other seasons SOA are minor components with strong POA emission from biomass burning. In most areas, simulated SOA mass concentrations are lower than those obtained by *Takemura et al.* [2005], which do not consider the SOA partitioning theory. They mainly overestimated SOA mass and number concentrations (Table 2). On the other hand, simulated values obtained by considering the SOA partitioning theory are close to in situ observations. In our simulation SOA formed from isoprene is not included, whereas *Henze and Seinfeld* [2006] included SOA formed from isoprene and calculated the difference in SOA mass concentrations between simulations with/without SOA from isoprene. In the Amazon basin, for example, simulated annual mean SOA mass concentrations near the surface differ by less than 1 μg m^{-3} between the two simulations. These differences can be smaller than the observational errors, so that it is difficult to conclude the differences between the result in this study and that by *Henze and Seinfeld* [2006] are meaningful. As for the global annual SOA production, our estimation is 6.74 Tg a^{-1}, whereas *Takemura et al.* [2005] used a value of 17.5 Tg a^{-1}.

[14] Figure 2 shows relative seasonal variations in SOA mass concentrations at three locations: Amazon

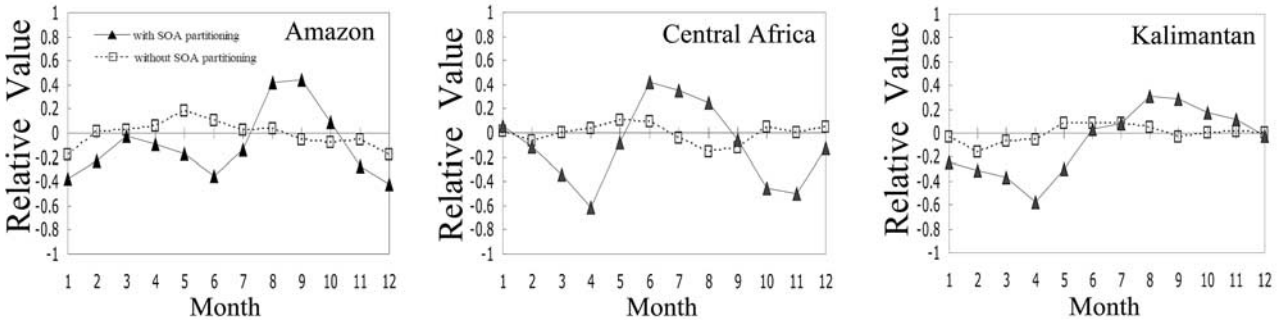

Figure 2. Relative seasonal SOA mass concentrations near surface in Amazon, central Africa, and Kalimantan. The x axis is month and the y axis is relative value.

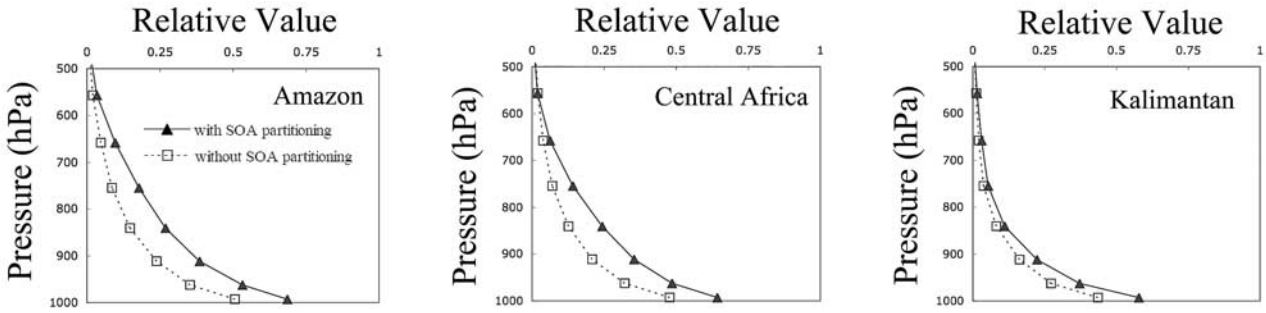

Figure 3. Relative vertical distributions of annual mean SOA mass concentrations in Amazon, central Africa, and Kalimantan. The *x* axis is relative SOA mass concentration and the *y* axis is air pressure (hPa).

(56°W–70°W, 1°N–10°S), central Africa (14°E–25°E, 4°N–4°S), and Kalimantan (110°E–118°E, 4°N–4°S), where the SOA production is relatively large [*Kanakidou et al.*, 2005]. Figure 2 indicates that the SOA concentrations obtained by considering the SOA partitioning theory have large seasonal variations because the monoterpene, POA and oxidant concentrations have different seasonal variabilities. Figure 3 shows relative vertical distributions in the SOA mass concentrations at three locations shown in Figure 2. Relative SOA masses are calculated as mass ratios to the surface SOA mass concentrations because the SOA mass concentrations with two simulations are very different as mentioned in the previous paragraph. At levels between 600 hPa and 1000 hPa and at all locations in Figure 3, the results with SOA partitioning are larger than that without SOA partitioning. These results may be predictable because simulated SOA without SOA partitioning are assumed to be emitted from surface. Although thus far the results cannot be compared to other locations, seasons and altitudes because of the lack of observations, the above comparison suggests that it is important to consider SOA-related processes in the model.

[15] Figures 4 and 5 also show results of seasonal variations in the (1) aerosol optical thickness (AOT) and (2) single scattering albedo (SSA) at the three locations shown in Figure 2. The three lines represent results from three schemes, i.e., with/without SOA partitioning theory and without SOA consideration. AOT differences among the three schemes are less than 0.1 in the Amazon and Kalimantan and less than 0.2 in central Africa. SSA differences are less than 0.03 in the Amazon and central Africa and less than 0.02 in Kalimantan. Seasonal changes in both AOT and SSA at all locations are similar among the three schemes, and there are no systematic monthly variations of both AOT and SSA. For AOT, while the contribution of SOA to the total AOT in wet season is close to almost 50%, that in dry season is much smaller and thus the annual mean becomes small. It is thus found that in these areas, differences in SSA and AOT by the three different SOA treatments are small, suggesting that at least the SOA from monoterpenes impact on the aerosol direct effect is weak.

[16] Figure 6 shows the vertical distributions of the annual and grid averaged cloud droplet number concentrations. The three lines show results from the three SOA schemes on the cloud droplet characteristics. In Figure 6, we plotted cloud droplet number concentrations in the height range from 500 to 950 hPa. In the present study, cloud droplet number concentrations are calculated through the parameterization based on the Köhler theory, depending on the updraft velocity, aerosol size distribution, and aerosol chemical properties. The simulated cloud droplet number concentrations are largely different near the surface because aerosol number concentrations, particularly the SOA number concentrations, are very different for these simulations. Compared to the differences in the AOT and SSA in Figures 4 and 5, the differences in cloud droplet number concentrations are much larger because SOA can act as CCN. However, in the middle troposphere of less than 500–600 hPa, these differences become almost zero, suggesting that the difference in monoterpenes emission and formations of SOA near the surface may not directly influence the cloud droplet formation in the middle and

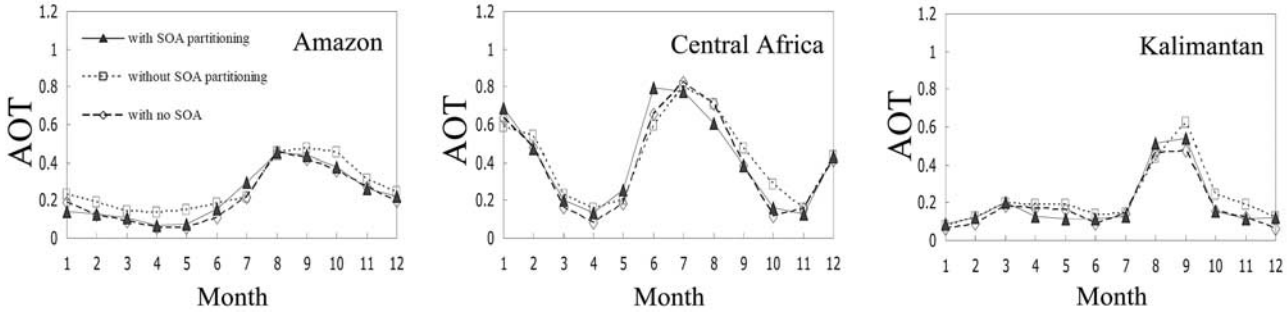

Figure 4. Seasonal aerosol optical thickness (AOT) in Amazon, central Africa, and Kalimantan. The *x* axis is month and the *y* axis is AOT.

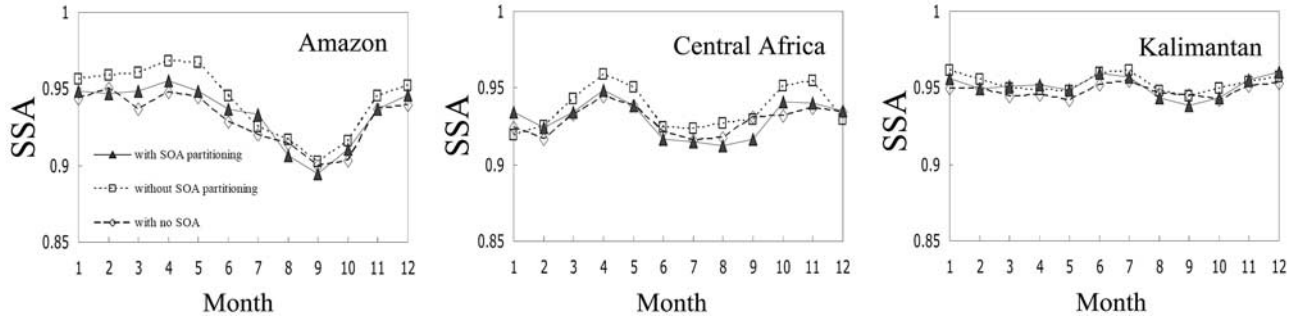

Figure 5. Seasonal single scattering albedo (SSA) in Amazon, central Africa, and Kalimantan. The *x* axis is month and the *y* axis is SSA.

upper troposphere. This suggests that SOA formed through monoterpene oxidation may not play an important role in the middle and upper troposphere.

[17] Figure 7 shows vertical distributions of the annual mean water cloud droplet effective radii (R_{eff}) of water clouds in the height range between 650 and 950 hPa for the three SOA schemes shown in Figures 4 and 5. The simulated R_{eff} are reflected by the simulated cloud droplet number concentrations in Figure 6. In SOA-rich land areas such as the Amazon and central Africa, the three lines are different, because the differences are caused by differences of SOA number concentrations due to difference of SOA mass yield. On the other hand, in the Kalimantan and ocean areas such as the east Pacific Ocean near Peru (82°W–98°W, 1°N–10°S) and east Atlantic Ocean near central Africa (0°E–8°E, 4°N–7°S), where lower cloud layers exist and R_{eff} are strongly affected by aerosols [*Takemura et al.*, 2005], the results obtained with/without the consideration of the SOA formation are similar. On the other hand the results obtained with/without the SOA partitioning theory are very different. The reason is that in the simulations without SOA partitioning theory, overestimated SOA in the ocean are transported from lands to oceans rather than formed over the ocean, according to the proposal by *Guenther et al.* [1995] that monoterpenes are not emitted from the ocean. The R_{eff} determines the cloud optical property, and therefore, the differences in R_{eff} among these schemes can affect the estimation of the aerosol indirect effect.

[18] Figure 8 shows the R_{eff} near the top of water clouds and compares three simulation results obtained with/without SOA partitioning theory and without SOA consideration with satellite observational data obtained from Advanced Very High Resolution Radiometer (AVHRR) [*Kawamoto et al.*, 2001]. The model results can be classified into three characteristic areas with different SOA distributions: (1) continental areas such as the Amazon and central Africa, (2) the East Pacific Ocean near Peru, East Atlantic Ocean near central Africa, and (3) desert areas such as Australia and the Namib Deserts. In the continental areas such as the Amazon and central Africa, where a large amount of SOA precursors are emitted [*Guenther et al.*, 1995], the simulated R_{eff} obtained by considering the SOA partitioning theory are larger than those obtained without considering the theory in the work of *Takemura et al.* [2005] by two or three micrometers. From Figure 7, the difference of simulated R_{eff} with/without SOA partitioning theory is caused by both the difference of SOA yield and different SOA formation processes. In the ocean, simulated R_{eff} obtained by considering the SOA partitioning theory are larger than those obtained without considering the SOA partitioning theory provided by *Takemura et al.* [2005]. In particular, in the East Pacific Ocean area near Peru and the east Atlantic Ocean near central Africa, simulated R_{eff} provided by *Takemura et al.* [2005] were very small because *Takemura et al.* [2005] predicted much larger cloud droplet number concentrations and aerosol number concentrations. The N_a-N_c parameterization with the Köhler theory tends to predict overestimated cloud droplet number concentrations especially for large aerosol number concentrations because of an ignorance of some kinetic processes such as condensational growth [e.g., *Chuang et al.*, 1997; *Nenes et al.*, 2001]. In these examples, simulated R_{eff} obtained by considering the

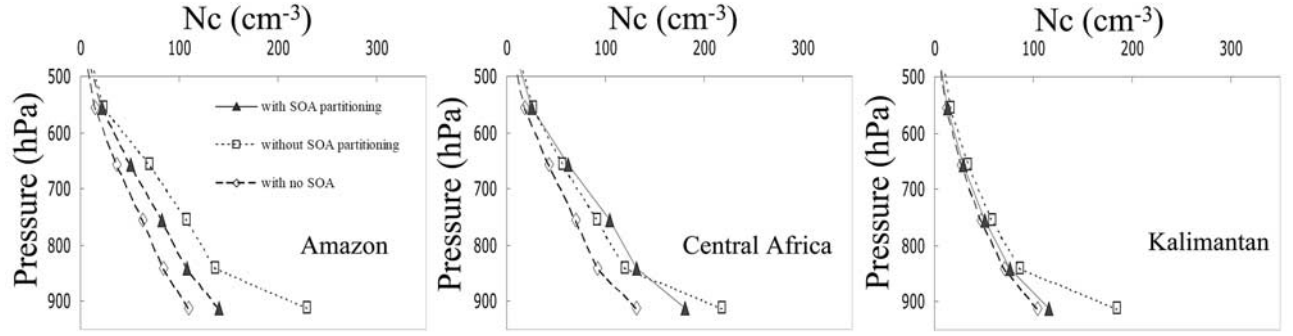

Figure 6. Vertical distributions of annual mean cloud droplet number concentrations (N_c(cm^{-3})) in Amazon, central Africa, and Kalimantan. The *x* axis is N_c (cm^{-3}) and the *y* axis is air pressure (hPa).

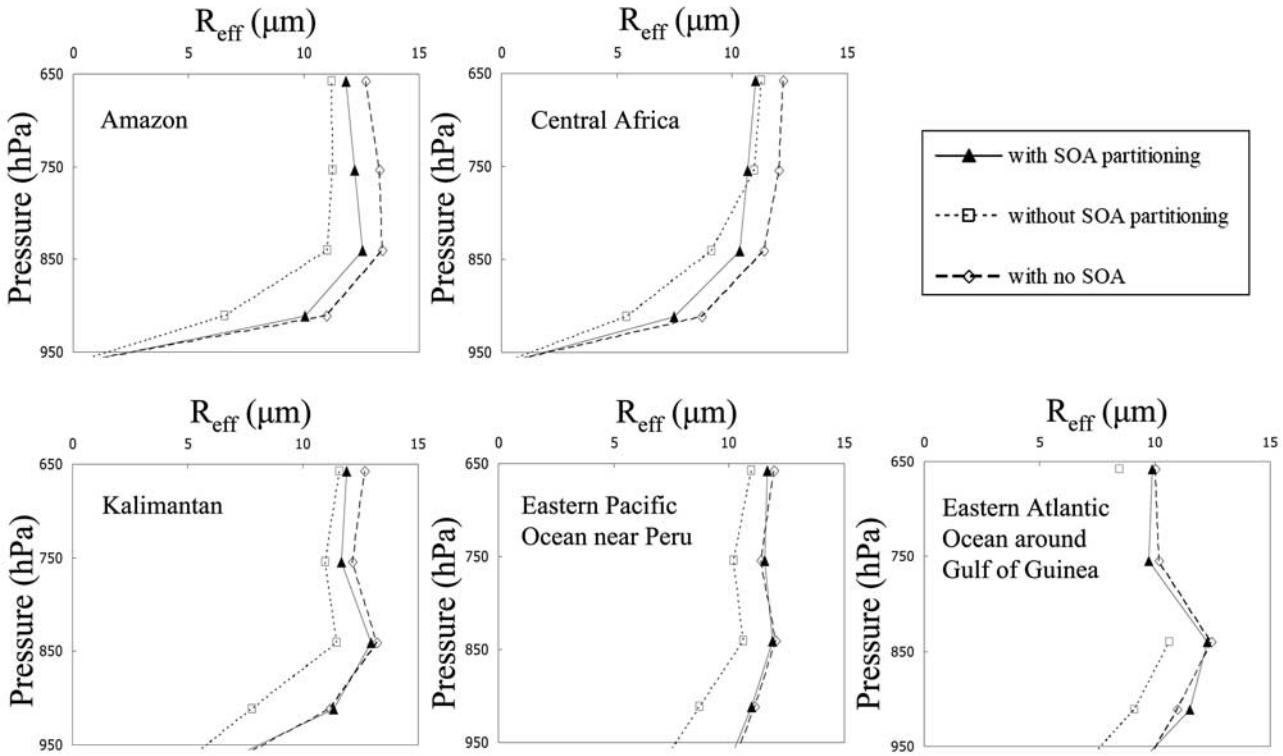

Figure 7. Vertical distributions of annual mean water cloud droplet effective radius (R_{eff} (μm)) in Amazon, central Africa, Kalimantan, eastern Pacific Ocean near Peru, and eastern Atlantic Ocean around Gulf of Guinea. The x axis is R_{eff} (μm) and the y axis is air pressure (hPa).

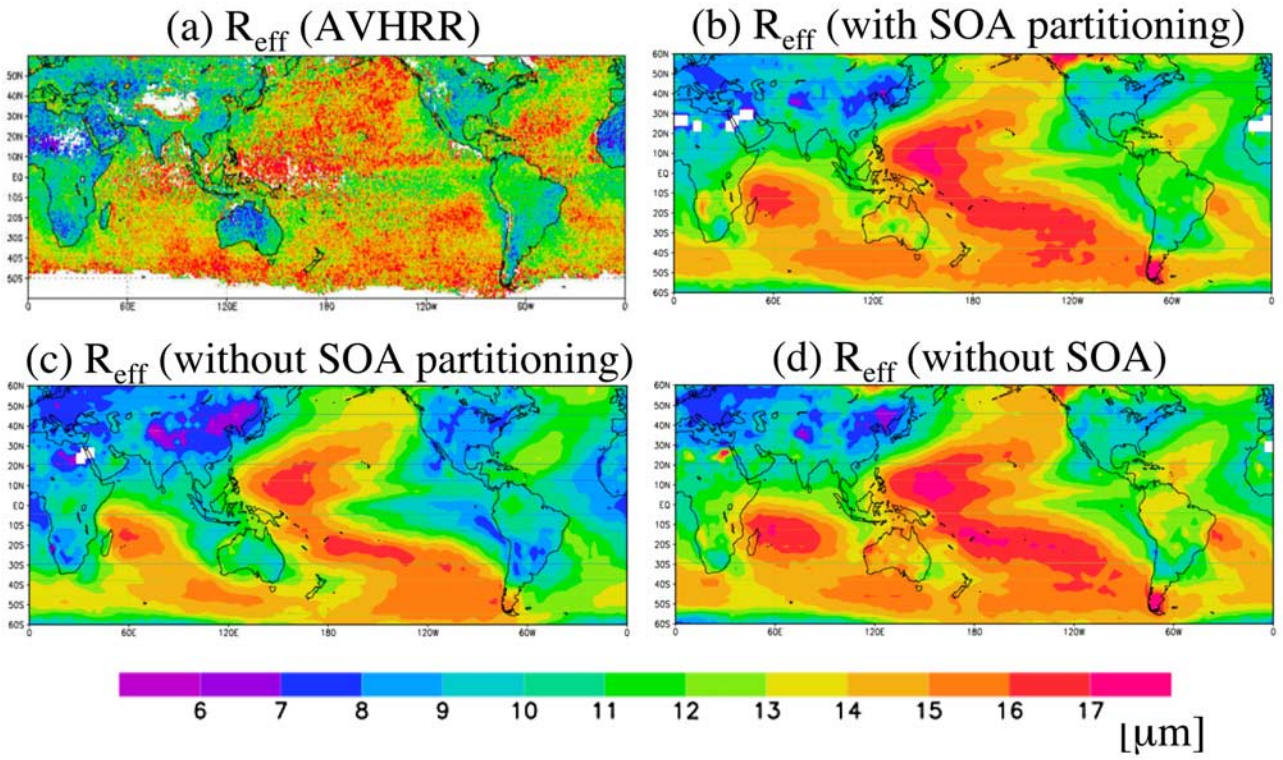

Figure 8. Annual mean water cloud droplet effective radius (R_{eff}) near the top of water clouds by (a) satellite measurement from AVHRR [*Kawamoto et al.*, 2001] and simulations (b) with and (c) without SOA partitioning theory and (d) without SOA treatments.

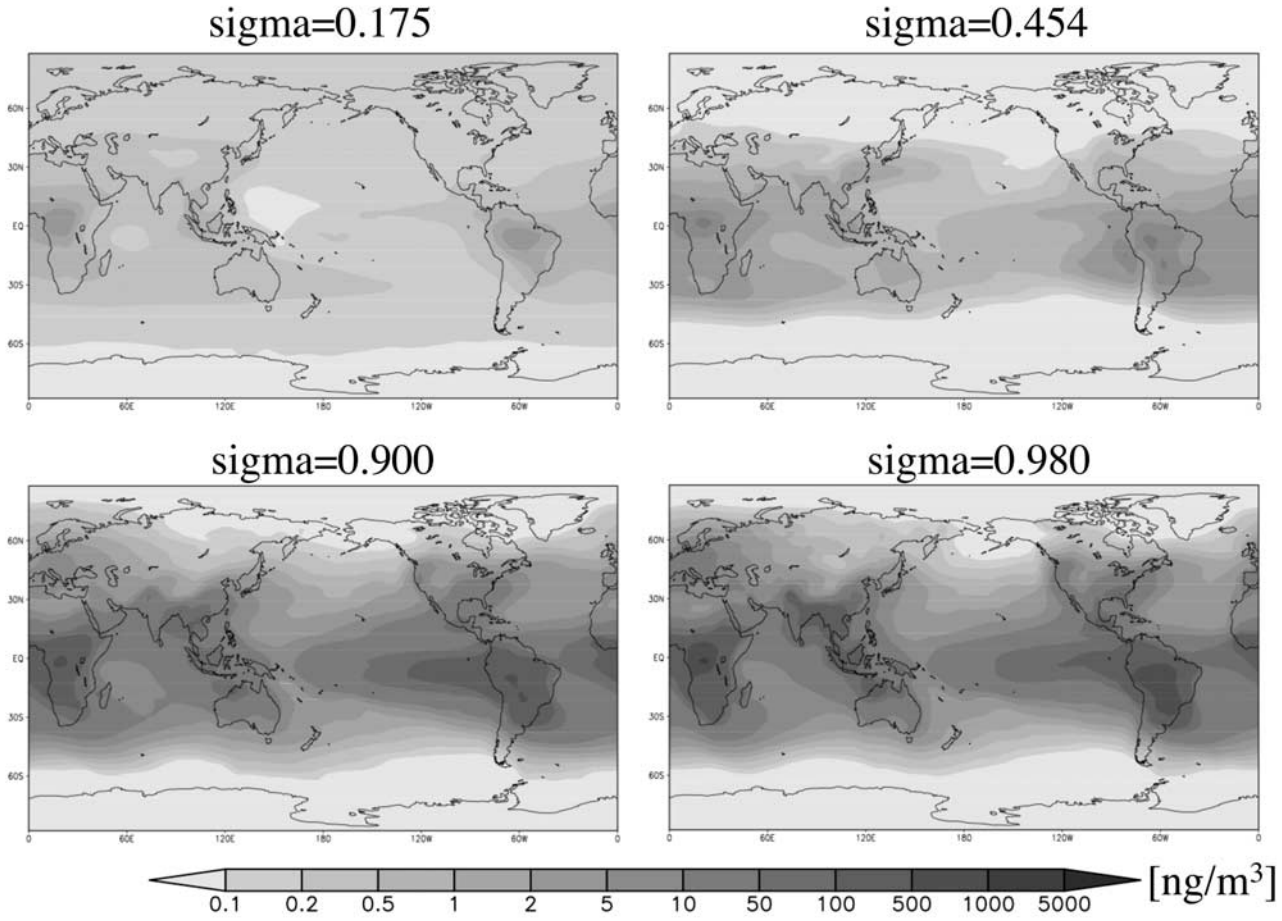

Figure 9. Vertical simulated annual mean SOA mass concentrations with SOA partitioning theory.

SOA partitioning theory are more comparable with values obtained from satellite remote sensing results than those obtained without considering the theory and than those obtained without SOA. In desert areas such as Australia and the Namib Deserts, however, simulated R_{eff} with the SOA partitioning theory are much larger than those obtained from satellite remote sensing results. Though there are many possibilities of overestimated R_{eff}, this larger value by simulation with SOA partitioning theory can be caused by a fact that satellite data from AVHRR and ADEOS-II/GLI images give smaller R_{eff}, particularly in desert areas (T. Y. Nakajima, personal communication, 2006). Because cloud microphysical remote sensing by satellite is difficult without enough cloud sample numbers, interpretation of the difference between model and observation should be left to future study. Another possibility of different R_{eff} may be caused by underestimation of N_c. Although this is highly uncertain, it means that it is possible to miss N_c formed from other SOA mechanism and from other SOA sources such as isoprene [e.g., *Claeys et al.*, 2004a, 2004b]. In practice, from Figures 8b–8d, we can find R_{eff} are large as SOA and N_c from SOA are small. In the Australia and Namib deserts, in particular, R_{eff} increase as SOA decrease. This suggests that SOA mainly determine R_{eff} in such areas. Additionally, near the deserts such as Australia and the Namib Deserts, there is a high possibility of SOA from isoprene as proposed by two reports: (1) a large amount of isoprene are emitted [*Guenther et al.*, 2006] and (2) *Henze and Seinfeld* [2006] showed SOA formed from isoprene increase SOA concentrations at higher altitudes including in the deserts such as Australia and the Namib Deserts. The SOA formed from isoprene can act as CCN and the inclusion may affect our results of N_c and R_{eff} without considering SOA from isoprene. However, it is difficult to assess this impact because the SOA partitioning theory does not give the ratio of condensation/nucleation.

[19] The direct radiative forcing of SOA is calculated as the difference in net fluxes between two results with and without SOA. The direct forcing is thus estimated to be -0.01 W m^{-2}, which is much smaller than -0.27 W m^{-2} for total organic carbon aerosols and -0.21 W m^{-2} for sulfate aerosol obtained by *Takemura et al.* [2005]. The contribution of the SOA forcing to the total direct forcing is consistent with that of AOT in Figure 4. Also the SOA indirect radiative forcing is calculated as the difference in the cloud radiative forcing between two results with and without

Table 3. Comparisons of Simulated SOA Burden, Production and Lifetime

	This Study	*Chung and Seinfeld* [2002]
Burden (Tg)	0.069	0.19
Production (Tg)	6.74	11.2
Lifetime (days)	3.74	6.2

Table 4. Annual POA Emission Fluxes

Products	This Study[a]	*Chung and Seinfeld* [2002][b]
Biomass burning (Tg a^{-1})	51.76	44.6
Fossil fuel (Tg a^{-1})	17.73	28.5
Total (Tg a^{-1})	88.2	81.0

[a]*Takemura et al.* [2005].
[b]*Liousse et al.* [1996].

SOA under the same meteorological conditions such as tropospheric temperature, wind and humidity. This method includes changes not only of R_{eff} but also of cloud water and of cloud fraction. That means we consider the first and the second aerosol indirect effect and the semidirect effect. The indirect effect for SOA is estimated as -0.19 W m^{-2}, which is much smaller in magnitude than -0.94 W m^{-2} for anthropogenic aerosols such as carbonaceous and sulfate aerosols in the work by *Takemura et al.* [2005] and range from -1 W m^{-} to -3 W m^{-2} for anthropogenic aerosols such as carbonaceous and sulfate aerosols in the work by *Lohmann and Feichter* [2005]. It is, therefore, concluded that the SOA have larger impact to the radiative forcing through indirect effect than through direct effect.

4. Comparison With Previous Studies

[20] In this section, we compare our simulated SOA distributions with other GCM results obtained using the SOA partitioning theory [*Chung and Seinfeld*, 2002; *Tsigaridis and Kanakidou*, 2003]. It is found from Table 3 that our results of global mean SOA burden, production and lifetime are smaller than those by *Chung and Seinfeld* [2002]. And the annual mean SOA mass concentrations at four vertical levels are compared in Figure 9. Figure 9 indicates that our SOA concentrations near the surface are very similar to the results obtained by *Chung and Seinfeld* [2002, Figure 5] in the tropics, while they are very different in northern industrialized regions such as Europe, China, and North America. In addition, the SOA distributions in the middle and upper troposphere obtained by *Chung and Seinfeld* [2002] are extended to the North Pole, whereas our SOA are less transported to the North Pole and stay around the tropics at all heights. Maximum values of the SOA mass concentration in the

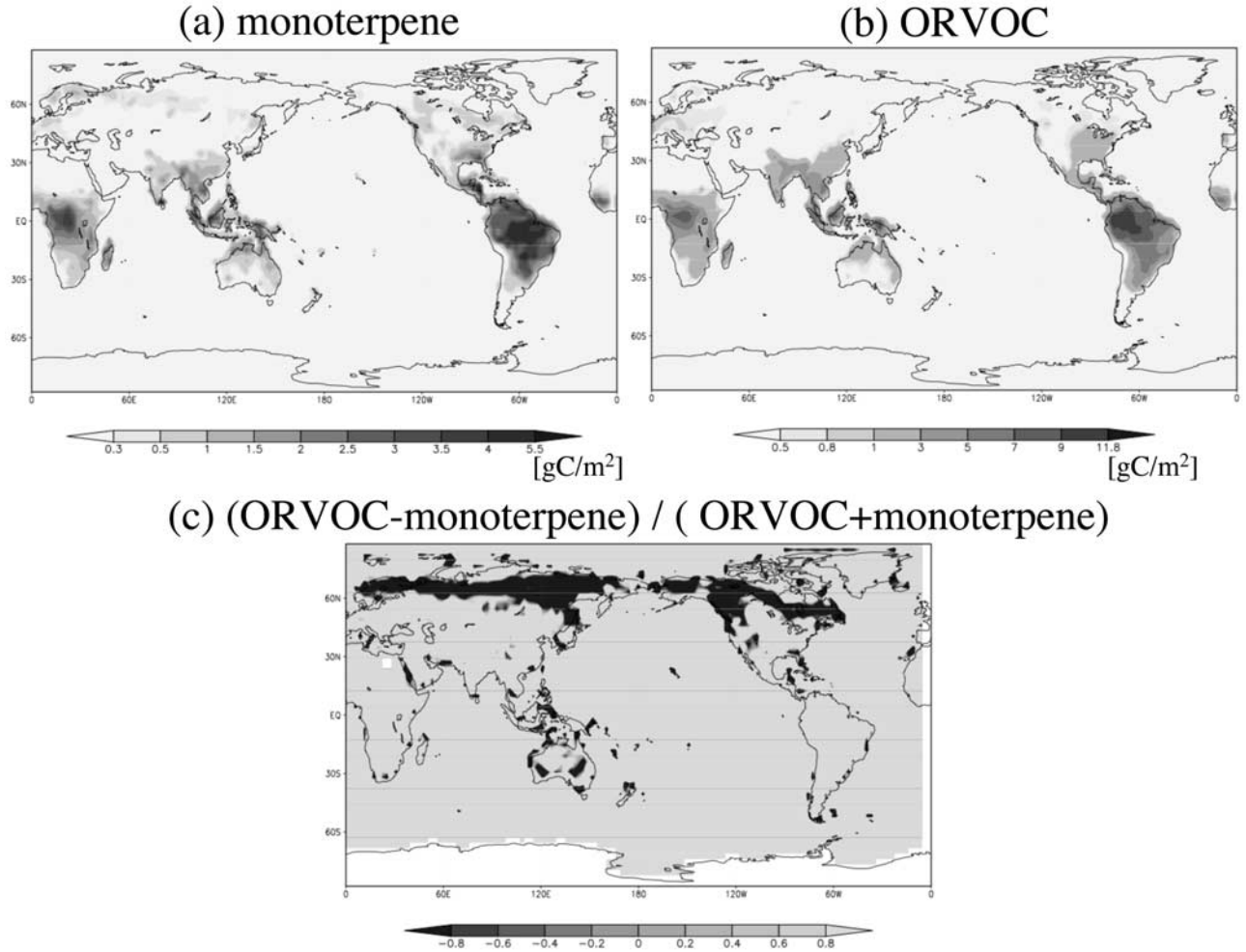

Figure 10. Annual mean (a) monoterpene emission data and (b) ORVOC emission data and (c) relative ratio of difference of monoterpene and ORVOC emission data to sum of monoterpene and ORVOC emission data.

Table 5. Predicted Relative SOA Burden as a Function of Relative POA Emission to Present Day[a]

POA	SOA
0.1	0.18
0.25	0.37
0.5	0.61
0.75	0.84
1	1

[a]Both values of POA emission and SOA burden in the present day are set to 1. We assumed that the relative POA emission in preindustrial era is approximately 0.1.

upper troposphere are much different between our results and that of *Chung and Seinfeld* [2002], i.e., 10 ng m^{-3} and 100 ng m^{-3}, respectively. These differences may be the results of not only model differences but also SOA treatments such as POA emissions differences, SOA precursor differences, different atmospheric lifetimes of generated monoterpene products, and SOA reversible/irreversible partitioning. Let us discuss these points in more detail.

[21] First, POA emissions in our study are based on the GEIA database, FAO, and several other original data sets [*Takemura et al.*, 2000, 2002, 2005] and those given by *Chung and Seinfeld* [2002, Figure 2] are based on *Liousse et al.* [1996] (Table 4). Table 4 shows that POA emissions from fossil fuel combustion in our study (17.73 Tg a^{-1}) are smaller than those in *Chung and Seinfeld* [2002] (28.5 Tg a^{-1}). Also we find that in our study POA emissions [*Takemura et al.*, 2005, Figure 1b] in Europe and China are smaller than those obtained by *Chung and Seinfeld* [2002, Figure 2]. Because SOA depend strongly on POA, we may conclude that the POA difference is the major source of the SOA concentration difference, particularly in industrial areas such as Europe, China, and North America, where POA emissions are very different among studies.

[22] Second, *Chung and Seinfeld* [2002] and *Tsigaridis and Kanakidou* [2003] added ORVOC to SOA precursors, unlike the present study. The ORVOC represent reactive VOC excluding isoprene and monoterpene and the emission rates are estimated as about 260 TgC a^{-1} [*Guenther et al.*, 1995]. Its characteristics are scarcely reported in the past other than by *Griffin et al.* [1999b], who assumed that 32% of ORVOC form particles, and therefore, its knowledge is highly uncertain. Figure 10 shows annual mean emission rates of monoterpene (Figure 10a) and ORVOC (Figure 10b), and the relative ratio of the difference of monoterpene and ORVOC emission rates to the sum of monoterpene and ORVOC (Figure 10c), i.e., the relative fraction of ORVOC. In Russia and Canada, the ratios of ORVOC to the total VOC are higher than those in other areas. This can be one of the reasons why the SOA distributions are different in different models especially in the Northern Hemisphere continental areas, where simulated SOA concentrations are much smaller in this study compared to other studies. Therefore we can hypothesize whether ORVOC are treated as SOA precursors or not is crucial for the SOA distributions.

[23] Third, we have to consider the fact that generated monoterpenes have high molecular weights and high polarity. Our assumption is that because of their high reactivities, they are removed from the atmosphere by some pathways within 20 min, which is one time step in our GCM computation. On the other hand, *Chung and Seinfeld* [2002] and *Tsigaridis and Kanakidou* [2003] treat them as longer lifetime products than the timescale of GCM time resolution. The different lifetimes of generated monoterpene products could result in different SOA mass distributions, especially in different SOA vertical distributions (Figure 9). It can be said that the treatment of generated monoterpene is crucial for determining the SOA distributions. In Figure 9 the simulated SOA mass concentrations near the surface in this study are comparable with some observations and are smaller the results by *Chung and Seinfeld* [2002, Figure 5]. In the middle and upper troposphere, our simulated SOA mass concentrations are smaller than their results. In these height in the Asia and the North Pacific Ocean, simulated SOA mass concentrations are generally underestimated [*Mader et al.*, 2002; *Maria et al.*, 2003; *Huebert et al.*, 2004; *Heald et al.*, 2005]. The underestimation of simulated SOA in middle and upper troposphere is the current issue.

[24] Fourth we assume irreversible partitioning of SOA, which means we do not consider reevaporation of SOA from particles. Unlike our study, *Chung and Seinfeld* [2002] and *Tsigaridis and Kanakidou* [2003] consider reversible partitioning of SOA and *Tsigaridis and Kanakidou* [2003] show the difference of SOA production with reversible/irreversible partitioning of SOA is very large under the assumption that generated monoterpenes can be transported. Hence in our results the difference of SOA production with reversible/irreversible reaction may be also large even though treatments of generated monoterpenes are different between our study and *Tsigaridis and Kanakidou* [2003]. However, it is difficult to estimate the magnitude of the particular difference caused by reversible/irreversible partitioning because the magnitude of the difference is dependent not only on the amount of SOA precursors including ORVOC and on the amount of POA distributions and emissions but also on the lifetime of the generated monoterpenes.

5. Implications of SOA Levels in the Preindustrial Era

[25] We consider SOA production in the preindustrial era. When we estimate the aerosol direct and indirect effects due to human activities, we need to know the magnitude of the aerosol production in the preindustrial era. This magnitude is highly unknown, so that each model has its own assumption. In general, natural SOA production in the preindustrial era is assumed to be the same as today (AeroCom: http://nansen.ipsl.jussieu.fr/AEROCOM/emission.html). In chamber experiments, however, the natural SOA production depends on POA, oxidants, and VOC concentrations [e.g., *Griffin et al.*, 1999b], and POA and oxidants concentrations are assumed to be smaller than today. As a result, the SOA concentrations in the preindustrial era, where POA concentrations are assumed to be smaller than today, are also expected to be smaller than today (Table 5). As well as past studies by *Chung and Seinfeld* [2002] and by *Tsigaridis and Kanakidou* [2003], this study shows that predicted SOA burdens in preindustrial era, where POA emissions are smaller by 90%, are smaller by 82% than

those in present day. These are important factors for estimating the aerosol direct and indirect effects.

6. Conclusions

[26] Comparisons of results from observations, other models, and our simulations with/without the consideration of the SOA partitioning theory lead to several findings regarding the influence of SOA on the radiation budget and the cloud field. First, SOA number concentrations can determine the cloud droplet effective radii near the top of water clouds in the tropics and can affect the estimation of the aerosol indirect effect. Second, SOA simulation results strongly depend on the POA concentration and on assumed POA emission data. Third, disregarding the dependence of the SOA formation on POA process may lead to a significant underestimation of the aerosol radiative effect if the SOA production level in the preindustrial era is assumed to be the same as the present-day level. The global annual mean production of SOA formed from monoterpene is evaluated in this study as 6.74 Tg a^{-1} and the global annual mean radiative forcings of the direct and indirect effects by SOA from monoterpene are calculated to be -0.01 and -0.19 W m^{-1}, respectively.

[27] **Acknowledgments.** We are grateful to K. Sudo of Nagoya University for providing chemical species data and to anonymous reviewers for their advice. This research was supported by Global Environment Research Fund B-4 of the Ministry of Environment, Japan; RR2002 project and data integration for the Earth Observation Project of Ministry of Science, Sports, and Culture; and JAXA/ADEOS-II GLI project.

References

Albrecht, B. A. (1989), Aerosols, cloud microphysics, and fractional cloudiness, *Science*, *245*, 1227–1230.

Artaxo, P., J. V. Martins, M. A. Yamasoe, A. S. Procopio, T. M. Pauliquevis, M. O. Andreae, P. Guyon, L. V. Gatti, and A. M. C. Leal (2002), Physical and chemical properties of aerosols in the wet and dry seasons in Rondonia, Amazonia, *J. Geophys. Res.*, *107*(D20), 8081, doi:10.1029/2001JD000666.

Berry, E. X. (1967), Cloud droplet growth by collection, *J. Atmos. Sci.*, *24*, 688–701.

Chuang, P. Y., R. J. Charlson, and J. H. Seinfeld (1997), Kinetic limitations on droplet formation in clouds, *Nature*, *390*, 594–596.

Chung, S. H., and J. H. Seinfeld (2002), Global distribution and climate forcing of carbonaceous aerosols, *J. Geophys. Res.*, *107*(D19), 4407, doi:10.1029/2001JD001397.

Claeys, M., et al. (2004a), Formation of secondary organic aerosols through photooxidation of isoprene, *Science*, *303*, 1173–1176.

Claeys, M., W. Wang, A. C. Ion, I. Kourtchev, A. Gelencser, and W. Maenhaut (2004b), Formation of secondary organic aerosols from isoprene and its gas-phase through reaction with hydrogen peroxide, *Atmos. Environ.*, *38*, 4093–4098.

Decesari, S. M., et al. (2006), Characterization of the organic composition of aerosols from Rondonia, Brazil, during the LBA-SMOCC 2002 experiment and its representation through model compounds, *Atmos. Chem. Phys.*, *6*, 375–402.

Ghan, S. J., L. R. Leung, R. C. Easter, and A. Abdul-Razzak (1997), Prediction of cloud droplet number in a general circulation model, *J. Geophys. Res.*, *102*, 21,777–21,794.

Griffin, R. J., D. R. Cocker, R. C. Flagan, and J. H. Seinfeld (1999a), Organic aerosol formation from the oxidation of biogenic hydrocarbons, *J. Geophys. Res.*, *104*, 3555–3567.

Griffin, R. J., D. R. Cocker, J. H. Seinfeld, and D. Dabdub (1999b), Estimate of global atmospheric aerosol from oxidation of biogenic hydrocarbons, *Geophys. Res. Lett.*, *26*, 2721–2724.

Guenther, A., et al. (1995), A global model of natural volatile organic compound emission, *J. Geophys. Res.*, *100*, 8873–8892.

Guenther, A., T. Karl, P. Harley, C. Wiedinmyer, P. I. Palmer, and C. Geron (2006), Estimates of global terrestrial isoprene emissions using MEGAN (Model of Emissions of Gases and Aerosols from Nature), *Atmos. Chem. Phys.*, *6*, 3181–3210.

Guyon, P., B. Graham, G. C. Roberts, O. L. Mayol-Bracero, W. Maenhaut, P. Artaxo, and M. O. Andreae (2003), In-canopy gradients, composition, sources, and optical properties of aerosol over the Amazon forest, *J. Geophys. Res.*, *108*(D18), 4591, doi:10.1029/2003JD003465.

Heald, C. L., D. J. Jacob, R. J. Park, L. M. Russell, B. J. Huebert, J. H. Seinfeld, H. Liao, and R. J. Weber (2005), A large organic aerosol source in the free troposphere missing from current models, *Geophys. Res. Lett.*, *32*, L18809, doi:10.1029/2005GL023831.

Henze, D. K., and J. H. Seinfeld (2006), Global secondary organic aerosol from isoprene oxidation, *Geophys. Res. Lett.*, *33*, L09812, doi:10.1029/2006GL025976.

Hoffer, A., A. Gelencser, M. Blazso, P. Guyon, P. Artaxo, and M. O. Andreae (2006), Diel and seasonal variations in the chemical composition of biomass burning aerosol, *Atmos. Chem. Phys.*, *6*, 3505–3515.

Hoffmann, T., J. R. Odum, F. Bowman, D. Collins, D. Klockow, R. C. Flagan, and J. H. Seinfeld (1997), Formation of organic aerosols from the oxidation of biogenic hydrocarbons, *J. Atmos. Chem.*, *26*, 189–222.

Huebert, B., T. Bertram, J. Kline, S. Howell, D. Eatough, and B. Blomquist (2004), Measurements of organic and elemental carbon in Asian outflow during ACE-Asia from the NSF/NCAR C-130, *J. Geophys. Res.*, *109*, D19S11, doi:10.1029/2004JD004700.

Jang, M., N. M. Czoschke, S. Lee, and R. M. Kamens (2002), Heterogeneous aerosol production by acid-catalyzed particle-phase reactions, *Science*, *298*, 814–817.

Jenkin, M. E. (2004), Modeling the formation and composition of secondary organic aerosol from α- and β-pinene ozonolysis using MCM v3, *Atmos. Chem. Phys.*, *4*, 1741–1757.

Kanakidou, M., et al. (2005), Organic aerosol and global climate modeling: a review, *Atmos. Chem. Phys.*, *5*, 1053–1123.

Kawamoto, K., T. Nakajima, and T. Y. Nakajima (2001), A global determination of cloud microphysics with AVHRR remote sensing, *J. Clim.*, *14*, 2054–2068.

Kroll, J. H., N. L. Ng, S. M. Murphy, R. C. Flagan, and J. H. Seinfeld (2005), Secondary organic aerosol formation from isoprene photooxidation under high-NOx conditions, *Geophys. Res. Lett.*, *32*, L18808, doi:10.1029/2005GL023637.

Lide, D. R., (Ed.) (2001), *CRC Handbook of Chemistry and Physics*, CRC Press, Boca Raton, Fla.

Liousse, C., J. E. Penner, C. Chuang, J. J. Walton, H. Essleman, and H. Cachier (1996), A global three-dimensional model study of carbonaceous aerosols, *J. Geophys. Res.*, *101*, 19,411–19,432.

Lohmann, U., and J. Feichter (2005), Global indirect aerosol effect: A review, *Atmos. Chem. Phys.*, *5*, 715–737.

Lohmann, U., J. Feichter, C. C. Chuang, and J. E. Penner (1999), Prediction of the number of cloud droplets in the ECHAM GCM, *J. Geophys. Res.*, *104*, 9169–9198.

Mader, B. T., C. Flagan, and J. H. Seinfeld (2002), Airborne measurements of atmospheric carbonaceous aerosols during ACE-Asia, *J. Geophys. Res.*, *107*(D23), 4704, doi:10.1029/2002JD002221.

Maria, S. F., L. M. Russell, B. J. Turpin, R. J. Porcja, T. L. Campos, R. J. Weber, and B. J. Huebert (2003), Source signatures of carbon monoxide and organic functional groups in Asian Pacific Regional Characterization Experiment (ACE-Asia) submicron aerosol types, *J. Geophys. Res.*, *108*(D23), 8637, doi:10.1029/2003JD003703.

Martins, G. M., D. W. Johnson, and A. Spice (1994), The measurement and parameterization of effective radius of droplets in warm stratocumulus clouds, *J. Atmos. Sci.*, *51*, 1823–1842.

Nakajima, T., M. Tsukamoto, Y. Tsushima, A. Numaguti, and T. Kimura (2000), Modeling of the radiative process in an atmospheric general circulation model, *Appl. Opt.*, *39*, 4869–4878.

Nenes, A., S. Ghan, H. Abdul-Razzak, P. Y. Chuang, and J. H. Seinfeld (2001), Kinetic limitations on cloud droplet formation and impact on cloud aldebo, *Tellus, Ser. B*, *53*, 133–149.

Pankow, J. F. (1994a), An absorption model of the gas/aerosol partitioning of organic compounds in the atmosphere, *Atmos. Environ.*, *28*, 185–188.

Pankow, J. F. (1994b), An adsorption model of the gas/aerosol partitioning involved in the formation of secondary organic aerosol, *Atmos. Environ.*, *28*, 189–193.

Penner, J. E., J. Quass, T. Storelvmo, T. Takemura, O. Boucher, H. Guo, A. Kirkervag, J. E. Kristjansson, and O. Seland (2006), Model intercomparison of indirect aerosol effects, *Atmos. Chem. Phys.*, *6*, 3391–3405.

Rissler, J., A. Vestin, E. Swietlicki, G. Fisch, J. Zhou, P. Artaxo, and M. O. Andreae (2006), Size distribution and hygroscopic properties of aerosol particles from dry-season biomass burning in Amazonia, *Atmos. Chem. Phys.*, *6*, 471–491.

Seinfeld, J. H., and S. N. Pandis (1998), *Atmospheric Chemistry and Physics: From Air Pollution to Climate Change*, John Wiley, New York.

Sudo, K., M. Takahashi, J. Kurokawa, and H. Akimoto (2002), CHASER: A global chemical model of the troposphere: 1. Model description, *J. Geophys. Res.*, *107*(D17), 4339, doi:10.1029/2001JD001113.

Takegawa, N., T. Miyakawa, Y. Kondo, J. L. Jimenez, Q. Zhang, D. R. Worsnop, and M. Fukuda (2006), Seasonal and diurnal variations of submicron organic aerosol in Tokyo observed using the Aerodyne aerosol mass sperctrometer, *J. Geophys. Res.*, *111*, D11206, doi:10.1029/2005JD006515.

Takemura, T., H. Okamoto, Y. Maruyama, A. Numaguti, A. Higurashi, and T. Nakajima (2000), Global three-dimensional simulation of aerosol optical thickness distribution of various origins, *J. Geophys. Res.*, *105*, 17,853–17,873.

Takemura, T., T. Nakajima, O. Dubovik, B. N. Holben, and S. Kinne (2002), Single scattering albedo and radiative forcing of various aerosol species with a global three-dimensional model, *J. Clim.*, *15*, 333–352.

Takemura, T., T. Nozawa, S. Emori, T. Y. Nakajima, and T. Nakajima (2005), Simulation of climate response to aerosol direct and indirect effects with aerosol transport-radiation model, *J. Geophys. Res.*, *110*, D02202, doi:10.1029/2004JD005029.

Textor, S., et al. (2006), Analysis and quantification of the diversities of aerosol life cycles within AeroCom, *Atmos. Chem. Phys.*, *6*, 1777–1813.

Tsigaridis, K., and M. Kanakidou (2003), Global modeling of secondary organic aerosol in the troposphere: A sensitivity analysis, *Atmos. Chem. Phys.*, *3*, 2879–2929.

Twomey, S. (1974), Pollution and the planetary albedo, *Atmos. Environ.*, *8*, 1251–1256.

Warneck, P. (2003), In-cloud chemistry opens pathway to the formation of oxalic acid in the marine atmosphere, *Atmospheric Environment*, *37*, 2423–2427.

Yu, J., H. E. Jeffries, and K. G. Sexton (1997), Atmospheric photooxidation of alkylbenzens—I. Carbonyl product analysis, *Atmos. Environ.*, *31*(15), 2261–2280.

D. Goto and T. Nakajima, Center for Climate System Research, University of Tokyo, Kashiwa, Chiba 277-8568, Japan. (teruyuki@ccsr.u-tokyo.ac.jp)

T. Takemura, Research Institute for Applied Mechanics, Kyusyu University, Kasuga, Fukuoka 816-8580, Japan.